Elsevier Editorial System(tm) for Water Research or its open access mirror
Manuscript Draft

Manuscript Number: WR55932R1

Title: Exploring multidecadal changes in climate and reservoir storage for assessing nonstationarity in flood peaks and risks worldwide by an integrated frequency analysis approach

Article Type: Research Paper

Keywords: Climate change; Reservoir regulation; Nonstationarity; Flood risk; Water management

Corresponding Author: Dr. Yanlai Zhou, PhD

Corresponding Author's Institution: University of Oslo

First Author: Yanlai Zhou, PhD

Order of Authors: Yanlai Zhou, PhD

Abstract: The changing climate and reservoir storage have a far-reaching influence on the nonstationarity in flood peaks worldwide, but the quantification of the relative contribution of each covariate (i.e., climate and reservoir storage) is fundamentally challenging especially under the time-varying mechanisms in statistical properties. This study proposed an integrated flood frequency analysis for assessing the impacts of changing climate and reservoir storage on the nonstationarity in flood peaks and flood risks worldwide. The 32 major river catchments covering more than 60% of hydro-meteorological observation stations and 70% of reservoir storage worldwide constituted the case study. The proposed three-faceted approach was explored systematically through: modeling the nonstationarity in global flood peaks, identifying the contribution of changing climate and reservoir storage to the nonstationarity of flood peaks, and quantifying the change in flood risks under the nonstationary condition. The findings pointed out that global flood trends varied from increasing +19.3%/decade to decreasing -31.6%/decade. Taking the stationary flood frequency analysis as the benchmark, the comparative results revealed that the flood risk in 5 rivers under the nonstationary condition in response to warming climate significantly increased (1% → 5%) over the historical period whereas the flood risk in 7 rivers in response to increasing reservoir storage largely reduced (1% → 0.5%). Despite the spatiotemporal heterogeneity of observations, the changes in flood peaks evaluated here were explicitly in lined with the changing climate and reservoir storage, supporting the demand for considering the nonstationarity of flood peaks and risks in social infrastructure planning and designing as well as water management.

Exploring multidecadal changes in climate and reservoir storage for assessing nonstationarity in flood peaks and risks worldwide by an integrated frequency analysis approach

Yanlai Zhou*

Department of Geosciences, University of Oslo, P.O. Box 1047 Blindern, N-0316 Oslo, Norway.

**Correspondence to*: Yanlai Zhou (yanlai.zhou@whu.edu.cn).

Abstract

The changing climate and reservoir storage have a far-reaching influence on the nonstationarity in flood peaks worldwide, but the quantification of the relative contribution of each covariate (i.e., climate and reservoir storage) is fundamentally challenging especially under the time-varying mechanisms in statistical properties. This study proposed an integrated flood frequency analysis for assessing the impacts of changing climate and reservoir storage on the nonstationarity in flood peaks and flood risks worldwide. The 32 major river catchments covering more than 60% of hydro-meteorological observation stations and 70% of reservoir storage worldwide constituted the case study. The proposed three-faceted approach was explored systematically through: modeling the nonstationarity in global flood peaks, identifying the contribution of changing climate and reservoir storage to the nonstationarity of flood peaks, and quantifying the change in flood risks under the nonstationary condition. The findings pointed out that global flood trends varied from increasing +19.3%/decade to decreasing –31.6%/decade. Taking the stationary flood frequency analysis as the benchmark, the comparative results revealed that the flood risk in 5 rivers under the nonstationary condition in response to warming climate significantly increased (1% → 5%) over the historical period whereas the flood risk in 7 rivers in response to increasing reservoir storage largely reduced (1% → 0.5%). Despite the spatiotemporal heterogeneity of observations, the changes in flood peaks evaluated here were explicitly in lined with the changing climate and reservoir storage, supporting the demand for considering the nonstationarity of flood peaks and risks in

social infrastructure planning and designing as well as water management.

Keywords: Climate change; Reservoir regulation; Nonstationarity; Flood risk; Water management

Nomenclature

Abbreviations

DOR	Degree of Regulation
EASM	East Asian Summer Monsoon
FAO	Food and Agriculture Organization
GAMLSS	Generalized Additive Models for Location, Scale and Shape parameters
GRDC	Global Runoff Data Centre
GSOD	Global Summary of the Day
PI-PW	Partial Information and Partial Weights
PIC	Partial Information Correlation
PMI	Partial Mutual Information
RI	Reservoir Index
SASM	South Asian Summer Monsoon
MI	Mutual Information
NASA	National Aeronautics and Space Administration
WCD	World Commission on Dams
WWF	World Wildlife Fund

Indices

t	index of time
h	index of anthropogenic covariates, from 1 to H
i	index of covariates, from 0 to I
j	index of reservoirs, from 1 to J
l	index of climate covariates, from 1 to L
m	index of dimensions in conditional vector Z, from 1 to M
n	index of sample observations, from 1 to N
k	index of neighbors permissible, from 1 to K

Parameters

H	number of anthropogenic covariates
I	number of covariates
J	number of reservoirs
K	number of neighbors permissible
L	number of climate covariates
M	number of dimensions in conditional vector Z
N	number of sample observations

Variables

A_j	catchment area controlled by j-th reservoir

$\mathrm{A_T}$	catchment area controlled by streamflow observation station
C_j	reservoir conservation pool of *j*-th reservoir
C_Z	contribution of climate covariate *Z*
C_P	contribution of anthropogenic covariate *P*
D	design life of infrastructure
DOR_j	degree of regulation corresponding to *j*-th reservoir
$\mathrm{DOR_T}$	degree of regulation corresponding to all reservoirs
$d(\cdot)$	density probability function in R software
d_k	number of observations whose distance from the covariate set **Z**
F_t	time-varying distribution function of flood peaks (y_t) at *t*-th time
$g(\cdot)$	log link function
P	potential covariate (e.g., reservoir index) to the system response
$P(\cdot)$	probability function
$\widehat{\mathrm{PIC}}$	estimated PIC ranging between [0, 1]
p_n	*n*-th sample observation of variable P
$p(\cdot)$	cummulative distribution function in R software
$q(\cdot)$	quantile function in R software
$r(\cdot)$	random number generator in R software
s_m	measure of spread for *m*-th dimension
T	return period corresponding to design life
T_{min}	minimal value of temperature
T_{mean}	mean value of temperature
T_{max}	maximal value of temperature
V_j	flood control capacity of *j*-th reservoir
$\mathrm{V_T}$	total flood control capacity of all reservoirs
$\overline{\mathrm{W}}_j$	average annual runoff (inflow) of *j*-th reservoir
$\overline{\mathrm{W}}_\mathrm{T}$	total average annual runoff of a river
X	system response (i.e., time-varying moment)
x_k	*k*-th observation of system response *X*
x_n	*n*-th sample observation of system response X
x_i^t	*i*-th covariate at *t*-th time
Y	random variable following the distribution F_t
y	observation value of flood peaks (y_t)
Z	climate factor consisting of precipitation and temperature
$\boldsymbol{Z}_{(-m)}$	climate covariate vector without the *m*-th covariate
$\boldsymbol{z_n}$	*n*-th sample observation of vector **Z**
α	vector of distribution parameters accounting for location and scale
α_{10}	constant in log link function for location
α_{20}	constant in log link function for scale
α_i^1	time-varying parameter account for location with *i*-th covariate
α_i^2	time-varying parameter account for scale with *i*-th covariate
β_m	measure of contribution of *m*-th covariate Z_m
$\beta_l(Z_l)$	contribution of *l*-th climate covariate Z_l
$\beta_h(P_h)$	contribution of *h*-th anthropogenic covariate P_h

ϵ_n	distance of conditional vector **Z**
θ_t	time-varying parameter vector at t-th time
θ_0	shape parameter in three-parameter distribution taken as a constant
μ	location parameter in the distribution of flood peaks
σ	scale parameter in the distribution of flood peaks
ν	shape parameter in the distribution of flood peaks

1. Introduction

Flood frequency analysis is one of the cornerstones in infrastructure projects' planning, design and management. The key assumption for conventional approaches to flood frequency analysis is that meteorological and hydrological datasets for use are independent and stationary while exhibiting respective identical distributions over time. Nevertheless, the validity of the stationarity assumption has already been disputed because climate change and anthropogenic activities (Aissia et al., 2014; Cheng and AghaKouchak, 2014; Schaller et al., 2016; Arheimer et al., 2017) have altered the statistical characteristics of hydrological process (Ashraf et al., 2018; Sarhadi et al., 2018). Infrastructure design projects using conventional methods based on the assumption of stationarity may not provide the water levels assumed for flood protection, water supply or hydropower generation over the design life since the nonstationarity would cause uncertainty and changes in the return period of a designed streamflow event (Forzieri et al., 2018). Consequently, in a changing environment, more in-depth researches are required to explicitly account for the nonstationarity in flood peaks. This research is expected to address an issue of topical interest, supporting societies to adapt to changing conditions in consideration of climate- and human-induced changes in flood peaks and risks (Montanari et al., 2013).

The scientific reason for exploring the flood risk of existing infrastructures and the need of using innovative approaches in support of designing future infrastructures are illustrated in Fig. 1. For the increasing flood trends, a design discharge Q_t has a return period T_0 under the stationary condition but corresponds to a much smaller return period T_1 under the nonstationary condition (Fig. 1(A)). For the same return period T_1, its corresponding design discharge is much larger under the nonstationary condition (Q_{t1}) than under the stationary condition (Q_0) (Fig. 1(B)). The relationship between flood risk (%), design life (*D*) and return period (T) can be formulated as $\mathrm{Risk}(\%) = 1 - \left(1 - \frac{1}{\mathrm{T}}\right)^{D}$. It shows that for a given return period T and the design life *D*, the flood risk is much larger under the nonstationary condition than under the stationary condition (Fig. 1(C)). In consequence, an infrastructure built for protecting a 100-year discharge under the stationary condition may only be possible to protect a 20-year discharge in the nonstationary condition under intensive climate and anthropogenic changes (Fig. 1(D)). Due to the assumption of the stationarity, for the increasing flood trends, design flood values would be underestimated, possibly raising future flood damages or dam failure risks (Fig. 1(D)). In contrast, for the decreasing flood trends, design flood values would be overestimated, potentially exerting unnecessary high costs on flood protection (Fig. 1(E)).

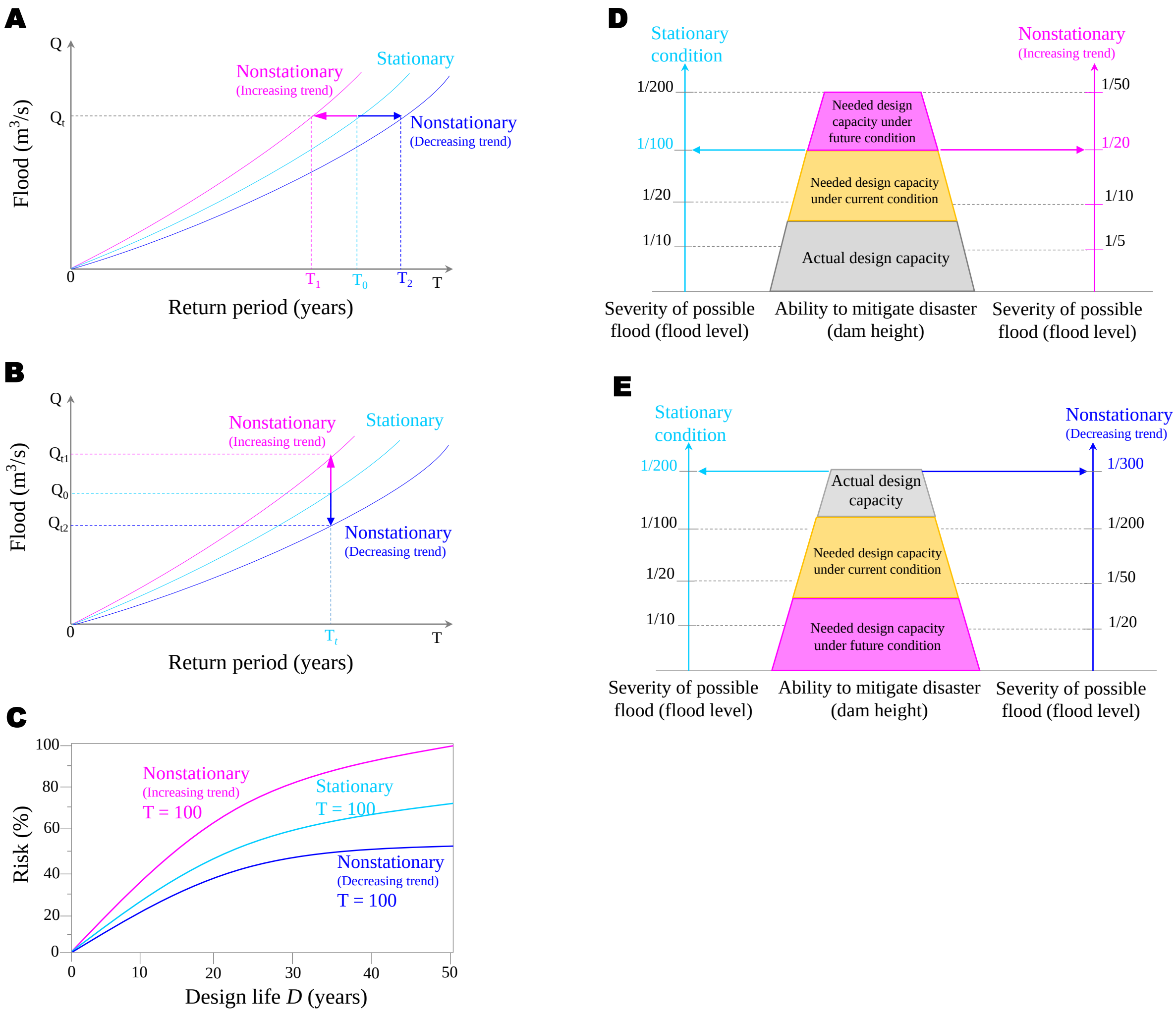

Fig. 1 Theoretical relationship under various scenarios. A-B. Relationship between flood and return period. C. Risk, design life and return period. D. Protection level compared between stationary and nonstationary conditions under increasing flood trends. E. Protection level compared between stationary and nonstationary conditions under decreasing flood trends.

This study is highly motivated by the global concern raised in recent years, that is, the frequency and intensity of flood events in consequence of climatic and anthropogenic changes (Milly et al., 2005; Mishra et al., 2012; Li et al., 2015) as well as drying antecedent conditions (Jones et al., 2010; Sharma et al., 2018) will bring damages to hydraulic infrastructures (Lins and Cohn, 2011; Hui et al., 2018). In general, infrastructures (e.g. dams, roads, sewers and stormwater drainage systems) were mostly designed using conventional methods based on the assumption of stationarity (Strupczewski et al., 2001; Milly et al., 2008). Given the observed increase of extreme events of precipitation, temperature and streamflow, the flood frequency analysis should be improved to account for climatic and anthropogenic changes, especially for hydraulic engineering and urban infrastructure design (Son et al., 2017; Ouarda and Charron, 2018; Sun et al., 2018). Haddeland et al. (2014) assessed the impacts of climate change, dams and water withdrawals on the hydrological cycle, global water resources and water supply and demand. Zhou et al. (2016) found that global reservoir capacity can induce 10%-70% variations of global surface water storage and the seasonal reservoir variations can be equal to the sum of snowmelt and soil moisture storage in several river catchments. Wasko and Sharma (2017) argued that increases in precipitation at higher temperatures and decreases in drying antecedent conditions correspond to increases in streamflow, which are closely associated with the sizes of catchments. Huss and Hock (2018) evaluated the impacts of global glacier decline on global glacier runoff for 56 large-scale glacierized catchments up to 2100. Yin et al. (2018) examined the sensitivity of the 99th percentile of precipitation and streamflow with temperature and concluded that storm runoff with a flash flooding mechanism would increase due to climatic and anthropogenic changes. Wasko et al. (2019) argued that decreases in drying antecedent conditions rather than increases in temperature would induce increased flooding. Worldwide climate and reservoir storage changes retreat and contribute to hydrological cycle changes, which raises major concerns over the global flood change. However global-scale assessments of the changing climate and reservoir storage as well as the resulting nonstationarity in flood peaks are rare.

The combination of climate and reservoir storage changes is imposing sharper and even long-running changes upon the nonstationarity of floods in the world's major rivers (Barichivich et al., 2018; Musselman et al., 2018; Willner et al., 2018). Therefore, quantifying the probability of floods that has changed over time is critical to risk management under a nonstationary condition as well as the understanding of historical impacts of global warming and reservoir storage changes on the flood nonstationarity. Hirabayashi et al. (2019) projected climate changes on flood risks at a global scale. Güneralp et al. (2015) offered a changing global pattern of flood and drought frequency under a warmer climate in the future. Best (2019) provided a global impact assessment of anthropogenic stressors on the world's 32 major rivers. From the perspective of a nonstationary climate, Sarhadi et al. (2018) quantified the spatial and temporal co-occurrence of climate stresses at a global scale. The aforementioned studies on the world's major rivers adopted only the temporal variable to model the parameters of the time-varying distribution for floods, yet they did not employ climatic and anthropogenic covariates of precipitation and temperature (climatic factors) as well as reservoir index (anthropogenic factor) to model the nonstationarity of flood peaks. These covariates would be more contributive to modeling the nonstationarity of flood peaks as compared with the temporal covariate, because they would quantify causal-physical mechanisms of flood nonstationarity (Liang et al., 2018; Xiong et al., 2018; Su et al., 2019; Yu et al., 2019).

Both the changing climate and reservoir storage are expected to have an impact on the nonstationarity of flood peaks; however, no consistent large-scale climate change and reservoir regulation signals in flood peak observations have been determined as yet due to the spatiotemporal distribution of limited hydrometeorological monitoring stations and reservoirs. According to the literature on the consistent changes (e.g., trend patterns) in flood peaks caused by global climate change, atmospheric blocking and reservoir regulation, the research gaps are described as follows. First, what are the patterns of flood peaks in the major rivers of the world? And what are the contributions of the changing climate and reservoir storage to the nonstationarity of flood peaks worldwide? Second, how to quantify the flood risk changes induced by the nonstationarity of floods in major rivers?

The goal of this study is to quantify the responses of the nonstationarity in flood peaks worldwide and flood risks to the changing climate and reservoir storage. The exploration was concentrated on three main foci. Firstly, the trend and the nonstationarity of flood peaks in each major river were detected and modeled by using the Generalized Additive Models for Location, Scale and Shape parameters (GAMLSS) method. Secondly, the contribution of multidecadal changes in climate and reservoir storage to the nonstationarity of flood peaks was identified by using the Partial Information and Partial Weights (PI-PW) method. Finally, the changes in flood risks under the nonstationary condition was quantified by using the time-varying distribution function. The 32 major river catchments covering more than 60% of hydro-meteorological observation stations and 70% of reservoir storage of the world constituted the case study.

The innovative nature of this study lies in proposing an integrated frequency analysis for the first time to quantify the multidecadal changes in climate and reservoir storage for assessing flood risks associated with the nonstationarity in flood peaks worldwide. The rest of this study was organized as below. Section 2 described data acquisition as well as data quality control. Section 3 introduced the methods used, including the GAMLSS method, the PI-PM method and the flood risk analysis. Section 4 showed the results of the methods employed to assess the nonstationarity in flood peaks and risks worldwide. Section 5 gave the conclusion.

2. Study area and materials

2.1. Study area and data acquisition

Fig. 2 illustrates the map of the world's 32 major rivers listed in order of drainage basin area as well as their principal climatic and anthropogenic factors. "Major" is specified as a river that possesses a large basin area (> 0.164 million km^2), a high mean annual streamflow (> 2,400 m^3/s) and a long length (>1,400 km) (Lehner et al., 2011; Best, 2019). This study adopted the numbers assigned to global top 32 rivers by the World Commission on Dams (WCD) according to basin size, mean annual streamflow and river length (Lehner and Grill, 2013; Lehner, 2013). Several reservoirs/dams were built along major rivers during the past century. A total of 6862 reservoirs, each with its storage capacity exceeding 10 million m^3, were investigated in this study.

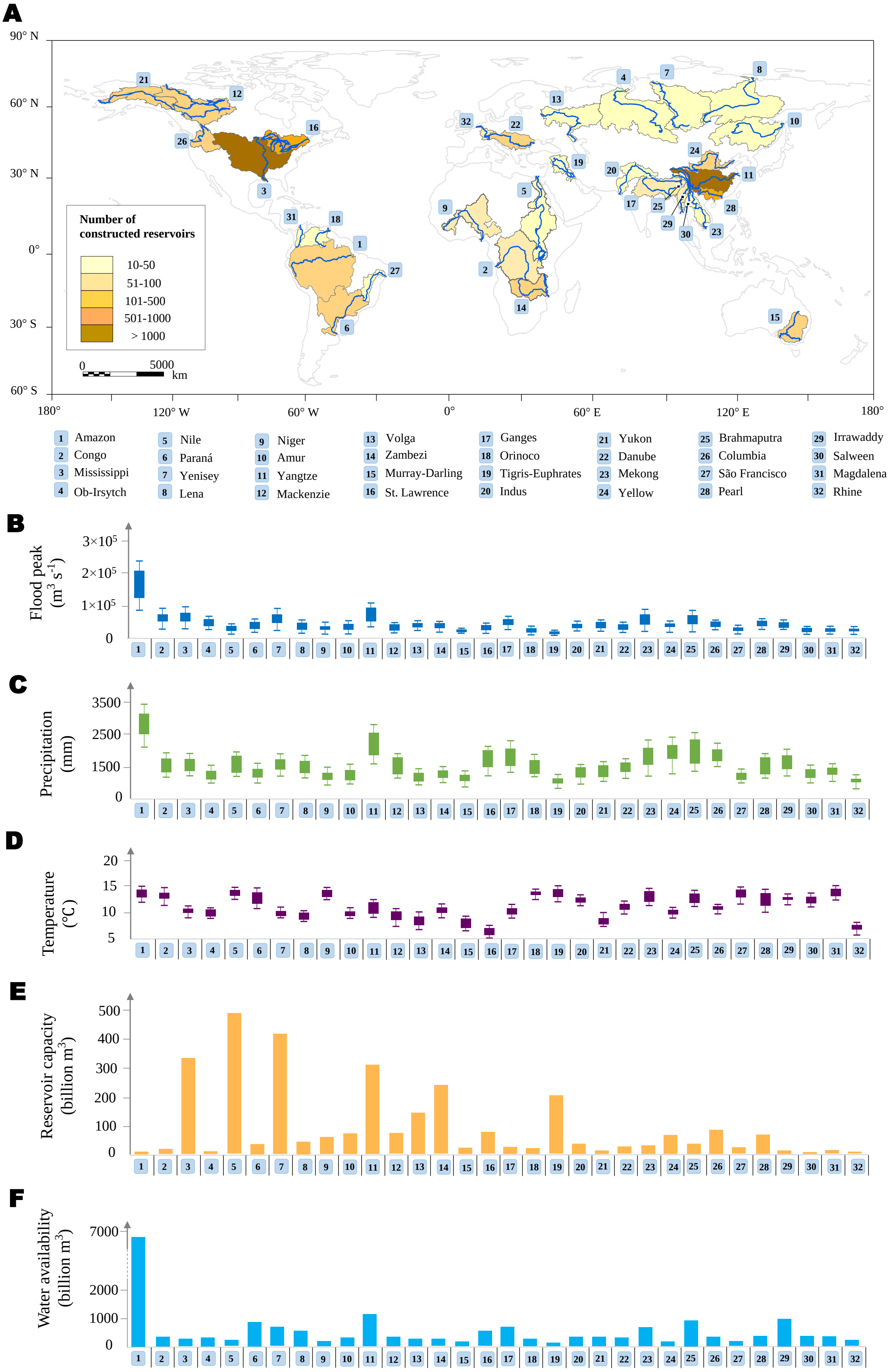

Fig. 2 Map of the world's 32 major rivers and the prelimary statistics of these river catchments. A. Map of the world's 32 major rivers. B. Flood peak over each catchment during

1931-2017. C. Accumulated annual precipitation (or annual precipitation total) over each catchment during 1931-2017. D. Annual average temperature over each catchment during 1931-2017. E. Reservoir capacity over each catchment up to 2017. F. Mean annual water availability over each catchment during 1931-2017. An inverse distance weighted method was used to convert gridded (1º × 1º) precipitation and temperature values into an average value over each catchment.

The world's major rivers are the cradles of human culture and civilization, supporting huge populations and diverse ecosystems (Najibi et al., 2018). The major rivers are mostly transboundary and play a key role in boosting regional collaborations yet ameliorating cross-boundary frictions. Being credited to the merits in nature, major rivers possess large water and hydropower resources in the world. The world's major rivers created tremendous societal benefits through food production, hydroelectricity generation and trade route development (Gernaat et al., 2017; Haer et al., 2020). However, flood events often cause significant losses of life and property in the basins of the world's major rivers (Tanoue et al., 2016; Paprotny et al., 2018; Hudson et al., 2019). Flood control and sustainable development of water resources under the changing environment is of vital importance globally, especially for countries whose prosperities are largely dependent on flood-level control and water-use efficiency (Dottori et al., 2018; De Koning et al., 2019; Krueger et al., 2019). Hence, it is interesting and important to conduct an impact assessment of the changing climate and reservoir storage on the nonstationarity of flood peaks and risks for the world's 32 major rivers.

Precipitation and air temperature (near-surface) datasets were extracted from the Global Summary of the Day (GSOD) datasets at a daily scale for the period of 1931-2017 and at a spatial scale of an 1º × 1º grid box, including 26592 gauging stations worldwide. Daily streamflow data for the period of 1931-2017 were extracted from the Global Runoff Data Centre (GRDC) datasets, covering 9543 observation stations and 225 river basins over the world (Fig. 3). Data of dams and reservoirs constructed during 1931-2017 in the world were obtained from the National Aeronautics and Space Administration (NASA), covering 6862 reservoirs/dams with a total storage capacity of approximately 6197 billion m^3 accounting for more than 75 % of the global storage capacity (Fig. 4). This study also used dam and reservoir data extracted from the Food and Agriculture Organization (FAO) for the same period. More details on the datasets used in this study can be found in the sources of the GRDC dataset (WWF, 2019; GRDC, 2020), the source of the GSOD dataset (https://resources.data.gov/) and the global dam and reservoir data (Lehner et al., 2011).

GSOD datasets are accessible on the website of the National Climate Data Center (https://catalog.data.gov/dataset/global-surface-summary-of-the-day-gsod). GRDC datasets are accessible on the website of the Global Runoff Data Centre (http://www.bafg.de/ GRDC/EN/Home/homepage_node.html). Dam and reservoir data are accessible on the websites of the NASA Earth Observing System Data and Information System (http://sedac.ciesin.columbia.edu/data/set/grand-v1-dams-rev01) and the FAO of the United Nations (http://www.fao.org/nr/water/aquastat/dams/index.stm).

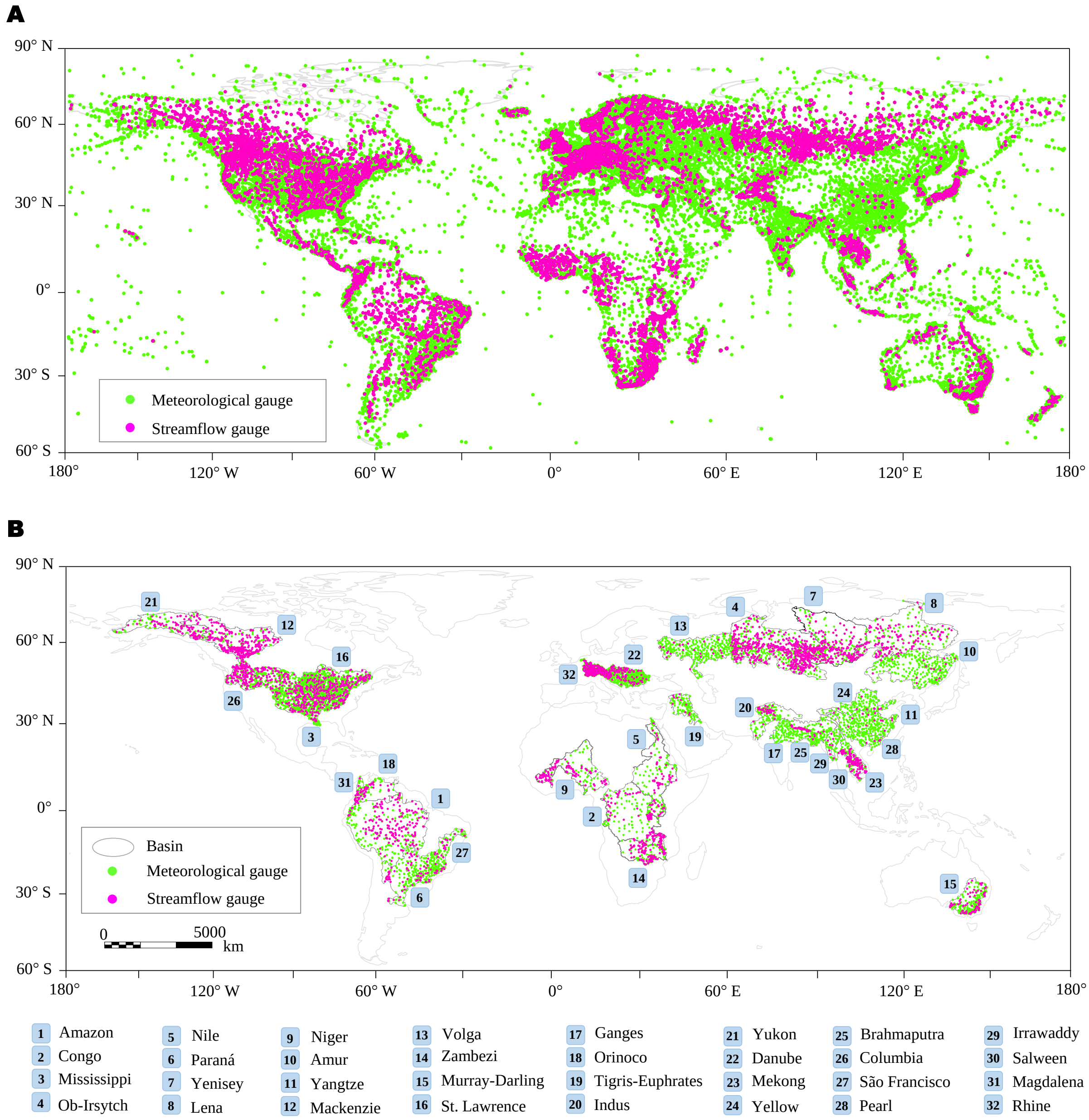

Fig. 3 Distribution of streamflow and meteorological observation stations. A. Observation stations in the globe. B. Observation stations located in the basins of 32 major rivers. Global discharge data were extracted from the GRDC datasets. Meteorological data were extracted from the GSOD datasets.

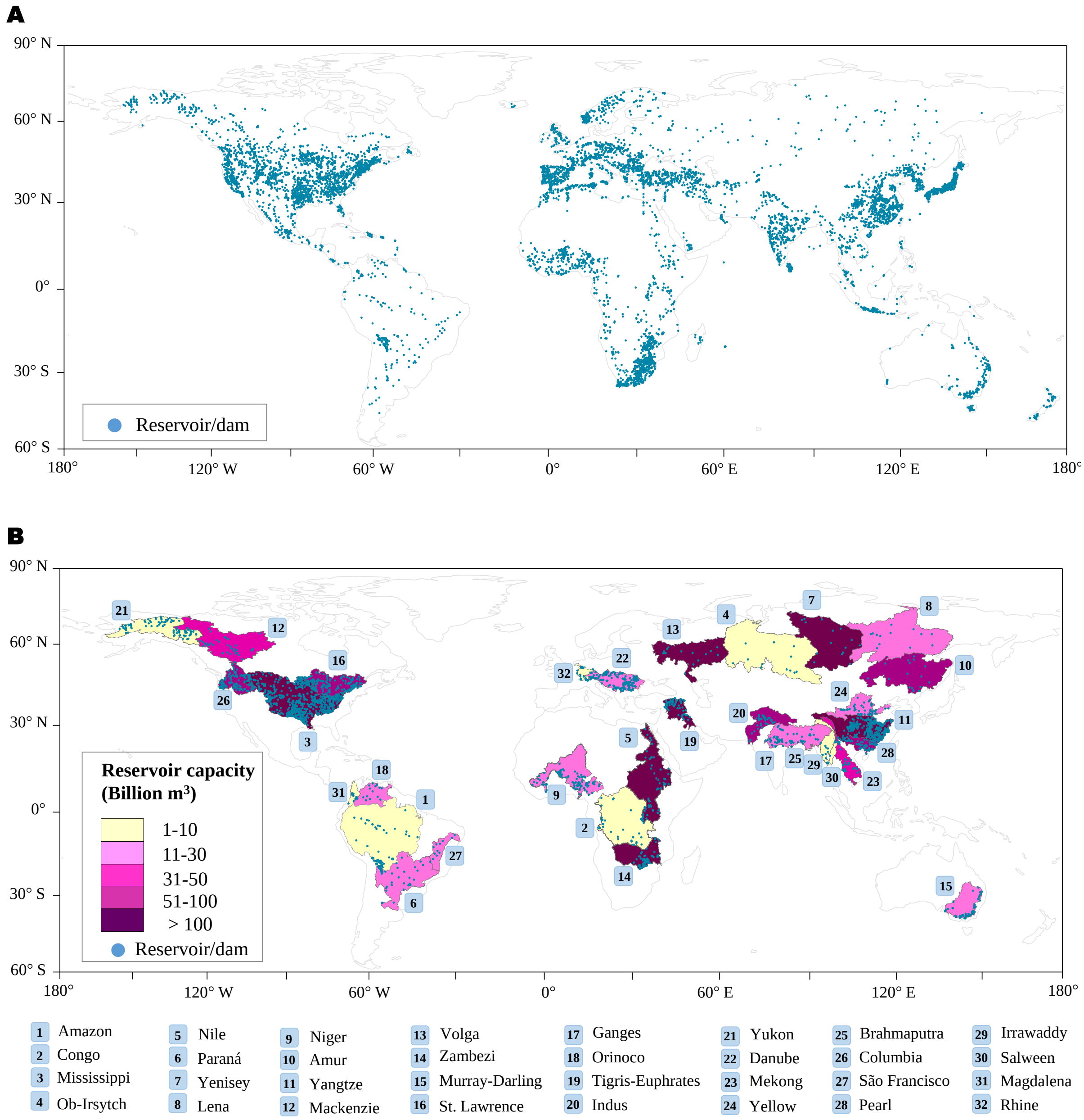

Fig. 4 Distribution of reservoirs/dams. A. Reservoirs/dams in the globe. B. Reservoirs/dams located in the basins of 32 major rivers. Reservoirs/dams data were extracted from the NASA Earth Observing System Data and Information System datasets and the FAO of the United Nations datasets.

2.2.Data quality control

All daily streamflow datasets used in this study are the observed datasets for preserving the characteristics of data affected by the changing climate and hydro-infrastructures (i.e., reservoir storage). During data pre-processing, this study conducted a quality control test. For each observation station, this study first prescreened temperature and precipitation data to identify obviously false data, for example, negative precipitation or $T_{\mathrm{max}} < T_{\mathrm{mean}}$ (or $T_{\mathrm{min}} > T_{\mathrm{mean}}$), where T_{min}, T_{mean} and T_{max} are the minimal, mean and maximal values of temperature. All reservoirs are included herein, with a total storage capacity of more than 0.01 billion m^3.

An inverse distance weighted method was used to convert gridded (1º × 1º) precipitation and temperature values into an average value over each catchment. The Kendall's tau correlation analysis was performed to identify the precipitation and temperature metrics the most important in explaining the variability of flood peaks. The daily precipitation (temperature) converted into the accumulated annual precipitation (annual average temperature) displayed a higher Kendall's tau correlation with flood peaks than the precipitation (temperature) at daily, monthly and seasonal scales. In this study, the accumulated annual precipitation and the annual average temperature of each catchment were considered as covariates. Additional details on regional flood frequency regarding the correlation analysis between flood peaks and precipitation and temperature at different time scales (daily, monthly, seasonal and annual) can be found in Villarini et al. (2009, 2011 and 2014), Vogel et al. (2011), Yan et al. (2017), Serago and Vogel (2018), Sharma et al. (2018), and Blöschl et al (2020).

The degree of regulation (DOR) index is introduced as a key component of studies on flow regulation driven by reservoir operation (Nilsson et al., 2005).

$$\mathrm{DOR}_j = \mathrm{C}_j / \overline{\mathrm{W}}_r \times 100\% \tag{1a}$$

$$\mathrm{DOR_T} = \sum_{j=1}^{J} \mathrm{C}_j / \overline{\mathrm{W}}_\mathrm{T} \times 100\% \quad (1b)$$

where C_j, $\overline{\mathrm{W}}_j$ and $\overline{\mathrm{W}}_\mathrm{T}$ denote the reservoir conservation pool, the average annual runoff (inflow) of the *j*-th reservoir and the total average annual runoff of a river, respectively. DOR_j and $\mathrm{DOR_T}$ are the degrees of regulation corresponding to the *j*-th reservoir and all reservoirs, respectively. It is noted that: first, $\mathrm{DOR} < 2\ \%$ (without regulation); second, $2\ \% \leqslant \mathrm{DOR} < 8\ \%$ (seasonal regulation); third, $8\ \% \leqslant \mathrm{DOR} < 20\ \%$ (incomplete annual regulation); fourth, $20\ \% \leqslant \mathrm{DOR} < 30\ \%$ (annual regulation); and fifth, $\mathrm{DOR} \geqslant 30\ \%$ (multi-year regulation). In the same sense here this study refers to rivers with a $\mathrm{DOR} \geqslant 2\ \%$ as "affected" rivers (Lehner et al., 2011).

3. Methods

The kernel framework of the integrated flood frequency analysis proposed in this study is illustrated in Fig. 5, involving three main parts. First, the time-varying distribution of flood peaks was modeled by using the GAMLSS method (Fig. 5(A)). Then, the contribution of climatic and anthropogenic drivers to the nonstationarity of flood peaks was identified by using the PI-PM method (Fig. 5(B)). Last, the changes in flood risks under the nonstationary condition were quantified by using the time-varying distribution function (Fig. 5(C)), as compared with those of the stationary condition. The methods used in this study were briefly introduced as follows.

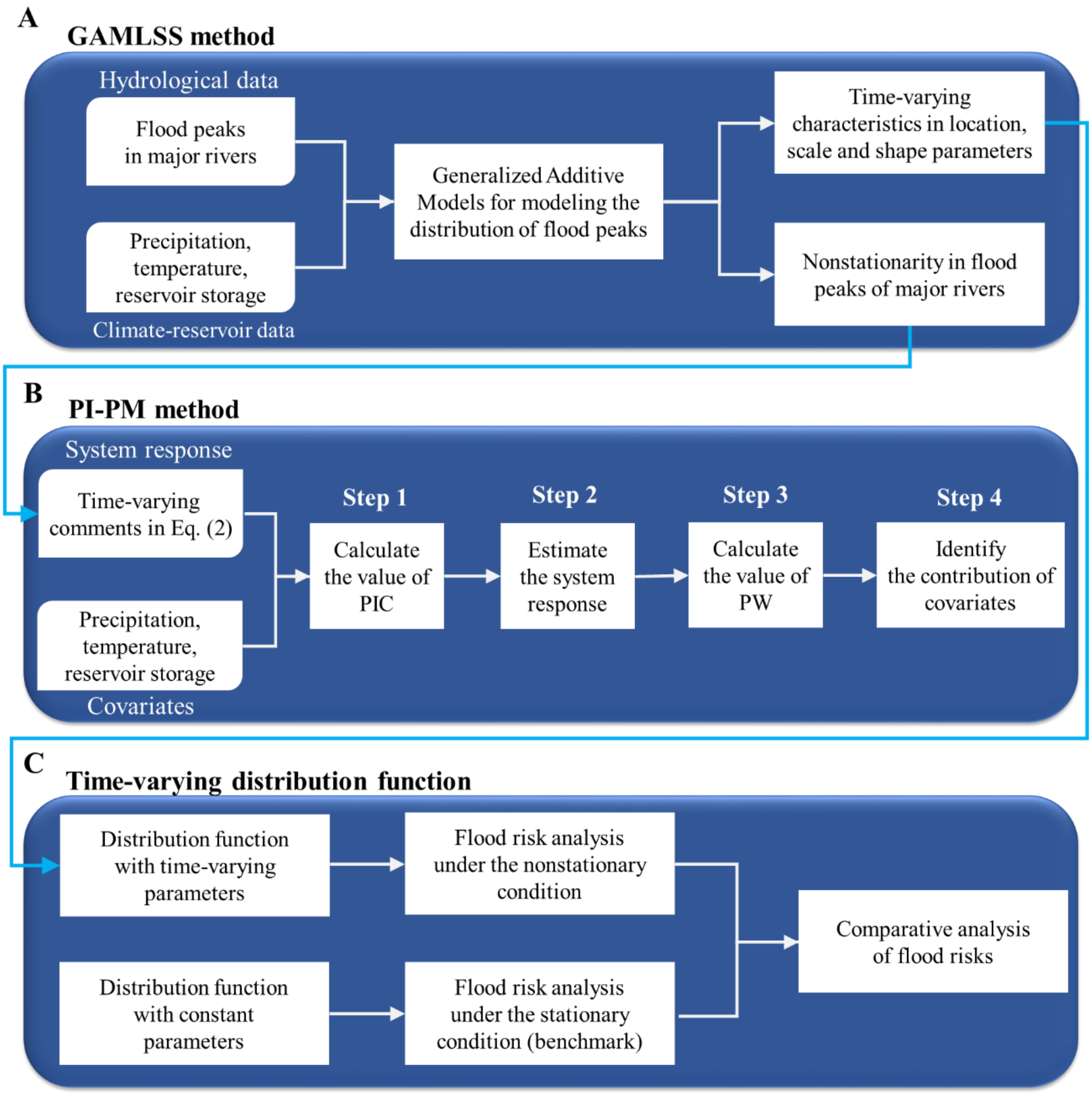

Fig. 5 Framework of the integrated flood frequency analysis proposed in this study. A. The Generalized Additive Models for Location, Scale and Shape parameters (GAMLSS) method for modeling the nonstationarity. B. The Partial Information and Partial Weights (PI-PW) method for identifying the contribution. C. The Time-varying distribution function for flood risk analysis.

3.1. Generalized Additive Models for Location, Scale and Shape parameters (GAMLSS)

Stationarity is defined as processes whose statistical properties such as the mean and variance are constant over time. In contrast, nonstationarity can simply be defined as processes that are not stationary but have statistical properties (e.g., mean and variance) that are deterministic functions of time (or covariates) (Koutsoyiannis, 2006; Milly et al., 2008; Lins and Cohn, 2011). The GAMLSS method proposed by Rigby and Stasinopoulos (2005) is used to model the nonstationarity of flood peaks by calculating the time-varying moments in the distribution. Consider the spatio-temporal heterogeneity of global flood patterns, eight probability distributions (Chebana et al., 2013; Gottschalk et al., 2013) are employed to fit the distributions of the flood peaks in this study (Table 1).

Table 1 Summary of distribution functions for fitting flood peaks.

Distribution function	**Probability distribution function (pdf)**	**Range**	**Parameters***
Weibull	$f(x\|\mu,\sigma) = \frac{\sigma x^{\sigma-1}}{\mu^{\sigma}} \exp\left[-\left(\frac{x}{\mu}\right)^{\sigma}\right]$	$x > 0$	$\mu > 0$ $\sigma > 0$
Gumbel	$f(x\|\mu,\sigma) = \frac{1}{\sigma} \exp\left\{-\frac{(x-\mu)}{\sigma} - \exp\left[-\frac{(x-\mu)}{\sigma}\right]\right\}$	$-\infty < x < +\infty$	$-\infty < \mu < +\infty$ $\sigma > 0$
Gamma	$f(x\|\mu,\sigma) = \frac{1}{(\mu\sigma^2)^{1/\sigma^2}} \frac{x^{(1/\sigma^2-1)} \exp[-x/(\mu\sigma^2)]}{\Gamma(1/\sigma^2)}$	$x > 0$	$\mu > 0$ $\sigma > 0$
Logistic	$f(x\|\mu,\sigma) = \frac{1}{\sigma}\left\{\exp\left[-\frac{(x-\mu)}{\sigma}\right]\right\} \cdot \left\{1 + \exp\left[-\frac{(x-\mu)}{\sigma}\right]\right\}^{-2}$	$-\infty < x < +\infty$	$-\infty < \mu < +\infty$ $\sigma > 0$
Normal	$f(x\|\mu,\sigma) = \frac{1}{\sqrt{2\pi}\sigma} \exp\left[-\frac{(x-\mu)^2}{2\sigma^2}\right]$	$-\infty < x < +\infty$	$-\infty < \mu < +\infty$ $\sigma > 0$
Lognormal	$f(x\|\mu,\sigma) = \frac{1}{\sqrt{2\pi}\sigma} \frac{1}{x} \exp\left[-\frac{(\ln x-\mu)^2}{2\sigma^2}\right]$	$x > 0$	$\mu > 0$ $\sigma > 0$
Generalised Extreme Value	$f(x\|\mu,\sigma,\nu) = \frac{1}{\sigma}\left[1 + \nu\left(\frac{x-\mu}{\sigma}\right)\right]^{(-1/\nu)-1} \cdot \exp\left\{-\left[1 + \nu\left(\frac{x-\mu}{\sigma}\right)\right]^{-1/\nu}\right\}$	$-\infty < x < +\infty$	$-\infty < \mu < +\infty$ $\sigma > 0$ $-\infty < \nu < +\infty$
Pearson type III	$f(x\|\mu,\sigma,\nu) = \frac{1}{\sigma\|\mu\nu\|\Gamma(1/\nu^2)} \left(\frac{x-\mu}{\mu\sigma\nu} + \frac{1}{\nu^2}\right)^{\frac{1}{\nu^2}-1} \cdot \exp\left[-\left(\frac{x-\mu}{\mu\sigma\nu} + \frac{1}{\nu^2}\right)\right]$	$\frac{x-\mu}{\mu\sigma\nu} + \frac{1}{\nu^2} \geq 0$	$\sigma > 0$ $\nu \neq 0$

*μ, σ and ν are the location, scale and shape parameters in the distribution of flood peaks.

When implementing the GAMLSS method, two-parameter distributions are commonly used to develop nonstationary models. The two-parameter distributions are less complicated. If the parameters of the distribution are best modeled by physical covariates, it is less likely that higher-order distributions are needed to explain the variability of flood peaks (Villarini et al., 2009 and 2011). Referring to Jiang et al. (2015) and Xiong et al. (2015a), only the location and scale parameters are considered as the time-varying parameters, where the shape parameter is taken as a constant.

$$g_1(\alpha_i^1) = \alpha_{10} + \sum_{i=1}^{I} \alpha_{1i}\, x_i^t \tag{2a}$$

$$g_2(\alpha_i^2) = \alpha_{20} + \sum_{i=1}^{\mathrm{I}} \alpha_{2i}\, x_i^t \tag{2b}$$

where $g(\cdot)$ is the log link function that recognizes the series of flood peaks may be skewed. $\alpha = (\alpha_i^1, \alpha_i^2)$ is the vector of distribution parameters accounting for location and scale, where $\alpha_i^1 = [\alpha_{10}, \alpha_{1i}]^{\mathrm{T}}$ and $\alpha_i^2 = [\alpha_{20}, \alpha_{2i}]^{\mathrm{T}}$ (i =1, 2, …, I). I is the number of covariates (i.e. explanatory variables). x_i^t is the *i*-th covariate at the *t*-th time.

In this study the accumulated annual precipitation and annual average temperature (climate covariates) as well as Reservoir Index (RI, anthropogenic covariate) are adopted as the covariates. An improved RI corresponding to each observation station is employed as the anthropogenic covariate described as follows.

$$\mathrm{RI} = \sum_{j=1}^{\mathrm{J}} \left(\frac{\mathrm{A}_j}{\mathrm{A}_\mathrm{T}}\right) \cdot \left(\frac{\mathrm{V}_j}{\mathrm{V}_\mathrm{T}}\right) \tag{3}$$

where A_j and A_T are the catchment areas controlled by the *j*-th reservoir and the observation station, respectively. V_j and V_T are the flood control capacity of the *j*-th reservoir and the total flood control capacity of all reservoirs in the observation station, respectively. J is the number of reservoirs.

The above-mentioned computations regarding the GAMLSS method were conducted in R (https://www.r-project.org/) by using the freely available GAMLSS package (D. M. Stasinopoulos et al. Instructions on how to use the GAMLSS package in R second edition, January.11.2008, available at http://www.gamlss.org).

3.2. Partial Information and Partial Weights (PI-PW)

The PI-PW method (Sharma and Mehrotra, 2014) provides higher flexibility and reliability in identifying predictors (independent variables or covariates) and quantifying their relative contributions without making assumptions about model structure or representation, in comparison to classical Mutual Information (MI) (Fraser and Swinney, 1986) and Partial Mutual Information (PMI) (Sharma, 2000). The PI-PW method that can quantify both linear and nonlinear correlations among multiple variables has been widely used in model input selection and contribution analysis in meteorological and environmental domains (Sharma et al., 2016). Therefore, the PI-PW method is adopted to account for the relative contribution of each covariate (climate or reservoir storage) to the nonstationarity in flood peaks, where the time-varying moments in Eq. (2), instead of flood peaks, are regarded as the system response variables. In other words, if the time-varying moments in Eq. (2) are taken as the system response, the PI-PW method will aim at identifying the contributions of three covariates to the nonstationarity of flood peaks. If flood peaks are taken as the system response, the PI-PW method will aim at identifying the contributions of three covariates to flood peaks. The former is different from the latter.

The implementation procedures of PI-PW for quantifying the relative contribution of each covariate to the nonstationarity of flood peaks consist of the following four steps.

Step 1: Calculate the value of Partial Information Correlation (PIC) between the dependent variable (i.e. each time-varying moment in Eq. (2)) and independent variables (i.e. climate and reservoir index covariates in Eq. (2)) using the following equation.

$$\widehat{\mathrm{PI}}(X,P|\boldsymbol{Z}) = \frac{1}{\mathrm{N}} \cdot \sum_{n=1}^{\mathrm{N}} log\left[\frac{f_{X|\boldsymbol{Z},P|\boldsymbol{Z}}(x_n,p_n|\boldsymbol{z_n})}{f_{X|\boldsymbol{Z}}(x_n|\boldsymbol{Z_n}) \cdot f_{P|\boldsymbol{Z}}(p_n|\boldsymbol{z_n})}\right] \tag{4a}$$

$$\widehat{\mathrm{PIC}} = \sqrt{1-\exp\left(-2\widehat{\mathrm{PI}}\right)} \tag{4b}$$

where $\widehat{\mathrm{PI}}(X,P|\boldsymbol{Z})$ is the estimated PI between variables (X,P) given the pre-existing covariate set $\boldsymbol{Z}$, where **Z** is the climate factor consisting of the accumulated annual precipitation and the annual average temperature of each catchment, X is the response (i.e., time-varying moment in Eq. (2)), and P is the potential covariate (e.g., reservoir index) to the response. $f_{X|\boldsymbol{Z}}(x_n|\boldsymbol{z_n})$, $f_{P|\boldsymbol{Z}}(p_n|\boldsymbol{z_n})$ and $f_{X|\boldsymbol{Z},P|\boldsymbol{Z}}(x_n,p_n|\boldsymbol{z_n})$ are the conditional marginal probability function estimates of X and P and the conditional joint probability function estimate of X and P given the pre-existing covariate set $\boldsymbol{Z}$, respectively. $(x_n, p_n, \boldsymbol{z_n})$, n=1, 2, …, N, are the sample observations of (X,P,Z). $\widehat{\mathrm{PIC}}$ is the estimated PIC ranging between [0, 1].

Step 2: Estimate the response X using a k-nearest-neighbor regression formulation. The weighted Euclidean distance is the most commonly used distance to identify neighbors to the covariate vector $\boldsymbol{Z}$ and is formulated below.

$$\epsilon_n^2 = \sum_{m=1}^{\mathrm{M}} \left(\frac{\beta_m(z_m - z_{n,m})}{s_m}\right)^2 \tag{5}$$

where ϵ_n is the distance of the conditional vector $\mathbf{Z}$ with M dimension, given the *n*-th data point z_n with M dimension. s_m is the measure of spread (e.g., standard deviation) for the *m*-th dimension. β_m is the measure of importance (i.e., contribution) of the *m*-th covariate Z_m.

And then the k-nearest neighbor conditional bootstrap and the regression estimator for estimating the response *X* are described below.

$$P(X|\boldsymbol{Z}) = \sum_{k=1}^{\mathrm{K}} \frac{1/d_k}{\sum_m 1/d_{k,m}} \quad (6a)$$

$$E(X|\boldsymbol{Z}) = \sum_{k=1}^{\mathrm{K}} \frac{x_k/d_k}{\sum_m 1/d_{k,m}} \quad (6b)$$

where $P(X|\boldsymbol{Z})$ and $E(X|\boldsymbol{Z})$ are the cumulative conditional probability distribution and the conditional expectation of X given the pre-existing covariate set **Z**, respectively. d_k is the number of observations whose distance from the covariate set **Z** is less than or equal to the distance to $\boldsymbol{z_k}$. x_k is the *k*-th observation of the variable X. The variable *k* ranges from 1 to K, and K is the maximal number of neighbors permissible. Additional details on the k-nearest neighbor conditional bootstrap (Eq. (6a)) and the regression estimator (Eq. (6b)) can be found in Lall and Sharma (1996).

Step 3: Compute the value of PW. Sharma and Mehrotra (2014) introduced an estimate of β_m in Eq. (5) by using the PIC metric in Eq. (4). The relationship between PW and PIC is formulated below.

$$\beta_m = PIC_{X,Z_m|\boldsymbol{Z}_{(-m)}} \frac{s_{X|\boldsymbol{Z}_{(-m)}}}{s_{Z_m|\boldsymbol{Z}_{(-m)}}} \quad (7)$$

where $\boldsymbol{Z}_{(-m)}$ is the climate covariate vector without the *m*-th covariate, and $S_{X|\boldsymbol{Z}_{(-m)}}$ and $S_{Z_m|\boldsymbol{Z}_{(-m)}}$ are the scaled conditional spread of residuals. More details on Steps 1-3 can be found in Sharma et al. (2016).

Step 4: Identify the contribution of covariates (climate Z and reservoir index P) to the nonstationarity (response X) in flood peaks by combining the time-varying moments in Eq. (2). The nonstationarity can simply be defined as processes whose statistical properties (e.g., mean and variance) are deterministic functions of covariates in Eq. (2). Hence, the contribution of each covariate can be calculated below.

$$C_Z = \sum_{l=1}^{\mathrm{L}} \beta_l(Z_l) \tag{8a}$$

$$C_P = \sum_{h=1}^{\mathrm{H}} \beta_h(P_h) \tag{8b}$$

where C_Z and C_P are the contributions of climate covariate Z and anthropogenic covariate P to the time-varying moment (i.e., system response), respectively. When the location and scale parameters are both time-varying moments (Eq. 2(a) and 2(b)), the value of C_Z (or C_P) is the average contribution. For an observation station the value of C_Z or C_P is the point contribution whereas for a whole catchment the value of C_Z or C_P is the average contribution over the catchment. In this study, the values of L and H are equal to two (accumulated annual precipitation and annual average temperature) and one (reservoir index), respectively. $\beta_l(Z_l)$ and $\beta_h(P_h)$ are the contributions of the l-th climate covariate Z_l and the h-th anthropogenic covariate P_h, respectively.

The above-mentioned computations with respect to the PI-PW method were conducted in R (https://www.r-project.org/) using the open-source R-software

NPRED (Sharma et al., 2016). The code of the NPRED package is available at http://hydrology.unsw.edu.au/download/software/NPRED.

3.3. Time-varying distribution function for flood risk analysis

After ascertaining the drivers and cause analysis for the nonstationarity of flood peaks, the next step is to quantify the flood risk changes associated with nonstationary conditions. According to the time-varying characteristic expressed in Eq. (2), the time-varying distribution function of flood peaks can be formulated below.

$$F_t = F(y_t|\theta_t) \tag{9a}$$

$$\theta_t = [\alpha_i^1, \alpha_i^2]^{\mathrm{T}} \;\; or \;\; [\alpha_i^1, \alpha_i^2, \theta_0]^{\mathrm{T}} \tag{9b}$$

where F_t is the time-varying distribution function of flood peaks (y_t) at the *t*-th time. For the two-parameter distribution the parameter vector θ_t consists of the location (α_i^1) and scale (α_i^2) parameters (i =1, 2, …, I) whereas for the three-parameter distribution the parameter vector θ_t consists of the location (α_i^1), scale (α_i^2) and shape (θ_0) parameters.

And then, the time-varying distribution function is employed to calculate the flood risk for each catchment and the flood risk is formulated below.

$$P(Y > y) = 1 - F(y_t|\theta_t) \tag{10}$$

where $P(\cdot)$ is the probability function. Y and y are the random variable following the distribution F_t and the observation value of flood peaks, respectively. Furthermore, the flood risk under the stationary condition (all parameters in the distribution of flood peaks are constant) is taken as the benchmark to conduct the comparative analysis.

The probability and risk computations were conducted in R (https://www.r-project.org/) by using the cumulative distribution function ($p(\cdot)$), density probability function ($d(\cdot)$), random number generator ($r(\cdot)$), quantile function ($q(\cdot)$), etc.

4. Results and discussion

This study centered on quantifying the nonstationarity of flood peaks and risks induced by the changing climate and reservoir storage in the basins of the world's 32 major rivers. The results and findings were presented and elaborated in three perspectives: the changing flood peaks worldwide (Section 4.1); the contribution of the changing climate and reservoir storage to the nonstationarity of flood peaks (Section 4.2); and the flood risk analysis under the changing climate and reservoir storage together with summarization (Section 4.3), shown as follows.

4.1. Changing flood peaks worldwide

A clear regional pattern (Fig. 6) in the trends of flood peaks across the basins of 32 major rivers was revealed based on our datasets using the Mann-Kendall nonparametric trend test. In comparison to the average value of flood peaks over the first time segment (1931-1960, baseline), regional flood trends changed from +19.3%/decade to –31.6%/decade (Fig. 6).

The spatial patterns of flood trends were classified into three groups. In the group containing the northern portion of North America, the central portion of South America, southern Africa and western Asia (Group (a) in Fig. 6(A)), about 67% of observation stations exhibited increasing trends in flood peaks and the local mean of flood peaks increased 9.4% per decade. In the group containing mid-southern Europe, Russia and China (Group (b) in Fig. 6(B)), around 78% of observation stations displayed declining trends in flood peaks and the local mean of flood peaks decreased 12.7% per decade. In the central portion of North America (Group (c) in Fig. 6(B)), about 71% of observation stations showed decreasing trends in flood peaks and the local mean of flood peaks decreased 6.9% per decade. Stepping from the second time segment (1961-1990, Fig. 6(A)) into the third time segment (1991-2017, Fig. 6(B)), both the increasing trends in Group (a) and the decreasing trends in Group (b) became more significant while the decreasing trends in Group (c) became weaker. As for the other major rivers, the trends of flood peaks at observation stations were less noticeable.

To be different from the previous researches (Wasko and Sharma, 2017; Yin et al., 2018), this study concentrated on ascertaining the trends of flood peaks directly, rather than on identifying the trends of flood peak scaling with extreme temperature. Do et al. (2017) analysed the trends in flood peaks using the GRDC datasets and found that the trends are more consistent at a continental scope, with downward trends for plenty of observation stations in western North America, the southern portion of South America, western Europe and Australia, whereas with upward trends for a large number of stations in eastern Europe, eastern North America, eastern South America and southern Africa. In this study, it is interesting to find that the flood peaks of the downward trends are prone to be larger as the catchment size and reservoir storage increase. From a global perspective, there are more observation stations with considerable declining trends in flood peaks than with considerable ascending trends based on the GRDC datasets investigated.

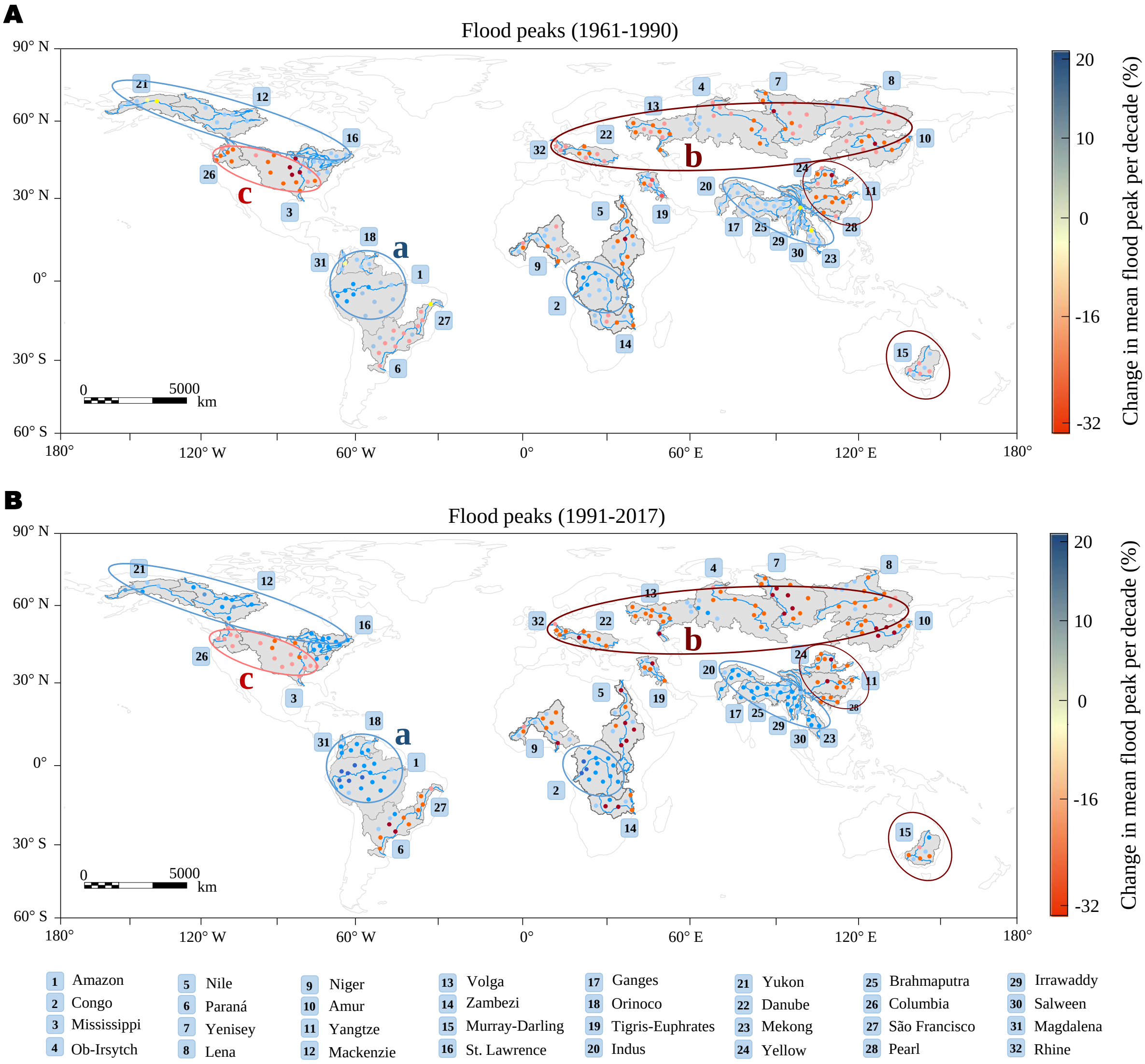

Fig. 6 Observed regional trends of flood peaks corresponding to the streamflow stations in the basins of the 32 major rivers during two periods (1961-1990 and 1991-2017), in comparison to the mean value of flood peaks over 1931-1960 (baseline). A. Trend of flood peaks during 1961-1990 using the Mann-Kendall nonparametric trend test. B. Trend of flood peaks during 1991-2017 using the Mann-Kendall nonparametric trend test. The white colour indicates stations with insufficient data or trends appearing insignificant at a significance level of 0.05.

In this study, 32 observation stations were specified to clarify these changes (Fig.

7). The consistency between the nonstationarity of flood peaks and three covariates of accumulated annual precipitation, annual average temperature and reservoir index was identified by using the GAMLSS method (see Section 3.1 in Methods). The flood peaks underwent two kinds (increasing & decreasing) of trend changes (Fig. 7(B)). In general, 81% (26/32) of the 32 major rivers shown significant nonstationarity in flood peaks. For the largely increasing ones (e.g. Amazon River, Fig. 7(A)), at least one substantial increase (+10%≤Δ<+30%) was found, where Δ was defined as the relative change of the average value of flood peaks over the period (1961-1990 or 1991-2017) in comparison to the average value of flood peaks over 1931-1960 (baseline). For the moderately increasing ones, two moderate upwards (+5%≤Δ<+10%) occurred. For the slightly increasing ones, at most one moderate plunge (Δ≤+5%) was found during the two periods. While for the strongly decreasing ones (e.g. Mississippi River, Fig. 7(A)), at least one strongly decreasing trend (Δ≤–30%) occurred. For the largely decreasing ones (e.g. Yenisey River, Fig. 7(A)), at least one substantial drop (–30%<Δ≤–10%) was found. For the moderately decreasing ones, two moderate plunges (–10%<Δ≤–5%) occurred. For the slightly decreasing ones, at most one moderate plunge was found during the two periods.

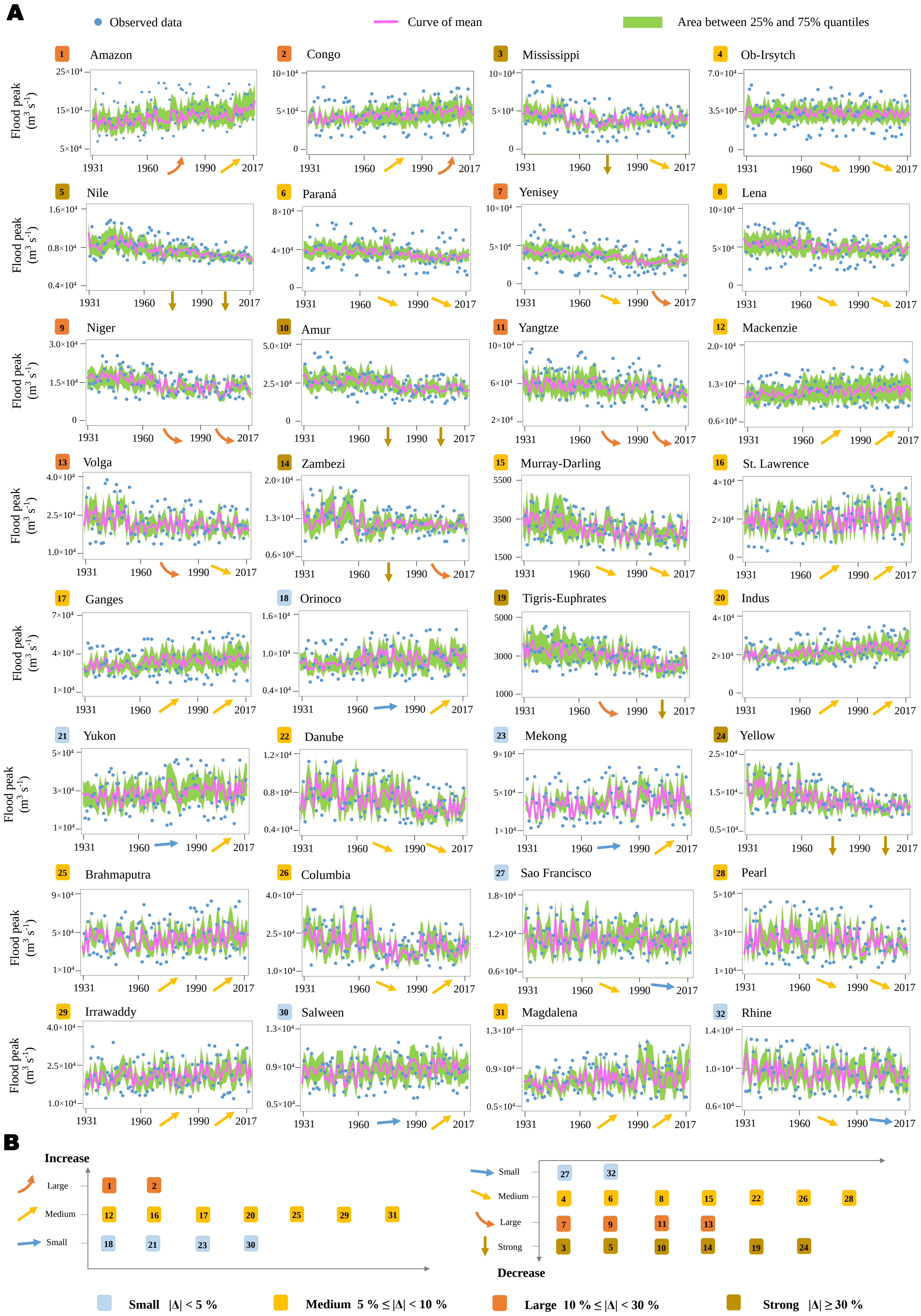

Fig. 7 Historical changes of flood peaks corresponding to the world's 32 major rivers (the observation stations) during two periods (1961-1990 and 1991-2017) under the

nonstationarity with the precipitation, temperature and reservoir index as covariates, in comparison to the mean flood peaks over 1931-1960 (baseline). A. Historical changes of flood peaks with the estimated interval between 25% and 75% quantiles. B. Overall trend of flood peaks during 1961-2017 using the Mann-Kendall nonparametric trend test at a significance level of 0.05. Δ is defined as the relative change of the average value of flood peaks over the period (1961-2017) in comparison to the average value of flood peaks over 1931-1960 (baseline).

4.2. Contribution of the changing climate and reservoir storage to the nonstationarity of flood peaks

And then, the PI-PW method was employed to further calculate the contribution of each covariate to the nonstationarity in flood peaks, where the time-varying moments in Eq. (2) were taken as the system response variables while the accumulated annual precipitation, annual average temperature and reservoir index were regarded as covariates. For each catchment the value of C_Z or C_P is the areal average contribution (see Section 3.2 in Methods). To explain the contribution of the changing climate and reservoir storage to the nonstationarity in flood peaks, this study paid special attention to three hotspots (regions (a), (b) and (c) in Fig. 8), owing to their significant and similar flood trends.

As compared with the other parts of North America, only the northern portion of North America in region (a) of Fig. 8 showed the raise in flood peaks corresponding to the increasing trend of the accumulated annual precipitation (Fig. S1), since snowmelt was closely associated with the flood formation. The datasets pointed out that the annual average temperature had a strong increase with > 0.7℃/decade (Fig. S2) while flood peaks in winter increased, reflecting earlier spring thaw and increasing snowmelt. In the northern South America of region (a) in Fig. 8, floods were mainly attributed to the summer rains and saturant soil moisture. The increasing summer precipitation plus soil moisture would make the scale and amount of flood peaks larger. Floods in the northern South America were in line with the increase in the accumulated annual precipitation (11.7%/decade during 1961-2017, Fig. S1), leading to the increase in the local mean of flood peaks. In the western Asia of region (a) in Fig. 8, the increase in the accumulated annual precipitation was closely associated with the atmospheric blocking raised meanwhile the declining pressure. For region (a), the contribution of climate change to the nonstationarity in flood peaks was significantly larger than that of reservoir regulation (Fig. 8). Hence, climate change had a dominant contribution to the nonstationarity in flood peaks of the major rivers in region (a).

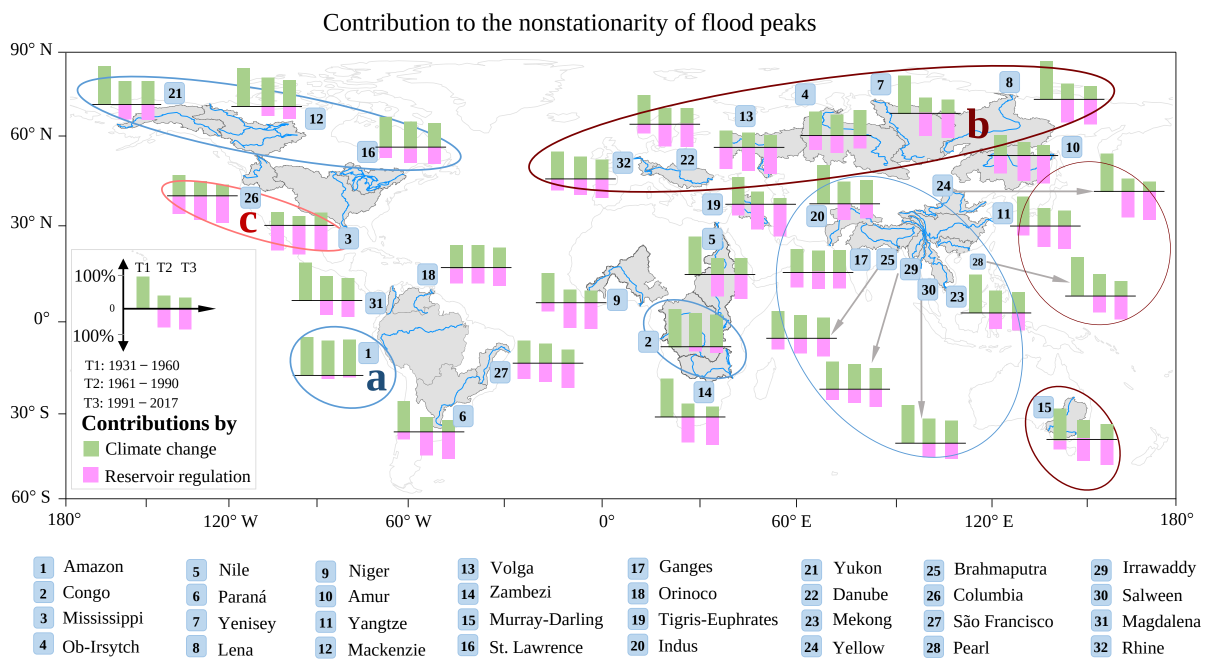

Fig. 8 Contribution of the changing climate and reservoir storage to the nonstationarity of flood peaks in the world's 32 major rivers during three periods (T1: 1931-1960, T2: 1961-1990; and T3: 1991-2017).

In the mid-southern Europe and Russia of region (b) in Fig. 8, a plunging trend of the accumulated annual precipitation covered 7 major rivers. Both the subtropical jet and the storm tracks in the mid-southern Europe moved toward the north (Blöschl et al., 2017; Hall and Blöschl, 2018; Mangini et al., 2018), resulting in a decrease in the accumulated annual precipitation (Fig. S1) and an increase in temperature associated with evapotranspiration (Frolova et al., 2017; Hodgkins et al., 2017; Blöschl et al., 2019), where the soil moisture would decrease notably, as much as -6.2%/decade. Particularly a noticeable accumulated annual precipitation decline occurred in Russia (Fig. S1), which was resulted from the decrease in the specific humidity. Furthermore, these rivers experienced a substantial increase in the number of reservoirs (Fig. S3) and the Degrees of Regulation (DOR, Fig. S4). The significant nonstationarity in flood peaks would easily appear in these major rivers, along which mega reservoirs/dams were put into flood control operation.

In China of region (b) in Fig. 8, the East Asian Summer Monsoon (EASM) flowing south-westward or south-eastward transported water vapour to East Asia and thus affecting the increase of precipitation in China. Previous studies (Winsemius et al., 2016; Wu et al., 2018) revealed that a significant contribution of the EASM than the South Asian Summer Monsoon (SASM) to the increase in precipitation throughout China, by around of +7.6% per decade (Fig. S1). The role (covariate) that dominated the contribution to the nonstationarity in flood peaks gradually shifted from climate change (1931-1960) to reservoir regulation (1991-2017) in 3 major rivers of China (region (b), Fig. 8).

In the central portion of North America of region (c) in Fig. 8, positive trends were found in the Mississippi River basin of the United States and the Columbia River basin of Canada. Both basins displayed considerable cooling trends (Fig. S2). Such cooling phenomena would be owing to intensive agricultural and land management activities (Yin et al., 2018). Observational and modelling studies demonstrated that agricultural and irrigation intensifications had the ability to decrease surface temperatures by increasing evapotranspiration (Mallakpour and Villarini, 2015; Schilling et al., 2015; Gao et al., 2019). Due to the sharp cooling/climate change, the Mississippi River and the Columbia River exhibited gradual upward trends of the accumulated annual precipitation between 1961 and 2017, by around +6.9% and +5.8% per decade respectively (Fig. S1). However, it is easy to find that the reservoir regulation had a dominant contribution to the nonstationarity in flood peaks of 2 major rivers in the central portion of North America (Fig. 8).

4.3. Flood risk analysis under the changing climate and reservoir storage

The time-varying distribution function was employed to quantify the flood risk under the nonstationary condition, where the flood risk analysis under the stationary condition served as the benchmark (see Section 3.3 in Methods). Taking the designed flood value with $P(X \geqslant x) = 1\ \%$ for example (Fig. 9), the increases in flood risks corresponding to 13 major rivers (40% = 13/32, colored in red) would be expected to increase the odds that these river basins experienced flood events simultaneously in consequence of increases in precipitation. Flood risks corresponding to 19 major rivers (60% = 19/32, colored in blue) would be expected to decrease because these river basins either had a large number of reservoirs/dams or experienced decreases in precipitation. Flood risks of 5 major rivers witnessed an increase from 0.01 (Return period = 100 years) to 0.05 (Return period = 20 years), whereas the flood risk of 7 major rivers witnessed a decrease from 0.01 (Return period = 100 years) to 0.005 (Return period = 200 years). It is easy to find that flood risks decreased sharply in the rivers (e.g. Mississippi, Yangtze and Columbia) whose reservoirs/dams were constructed with large flood control capacities, but flood risks increased dramatically in the rivers (e.g. Amazon, Ob-Irsytch and St. Lawrence) that underwent increasing precipitation and reservoirs/dams built here had small flood control capacities. The emergence of the changing climate and reservoir storage signals during 1961-2017 was particularly prominent according to the historical changes in flood risks. The results demonstrated that the difference in flood risk was statistically significant for 32 major rivers in the three periods.

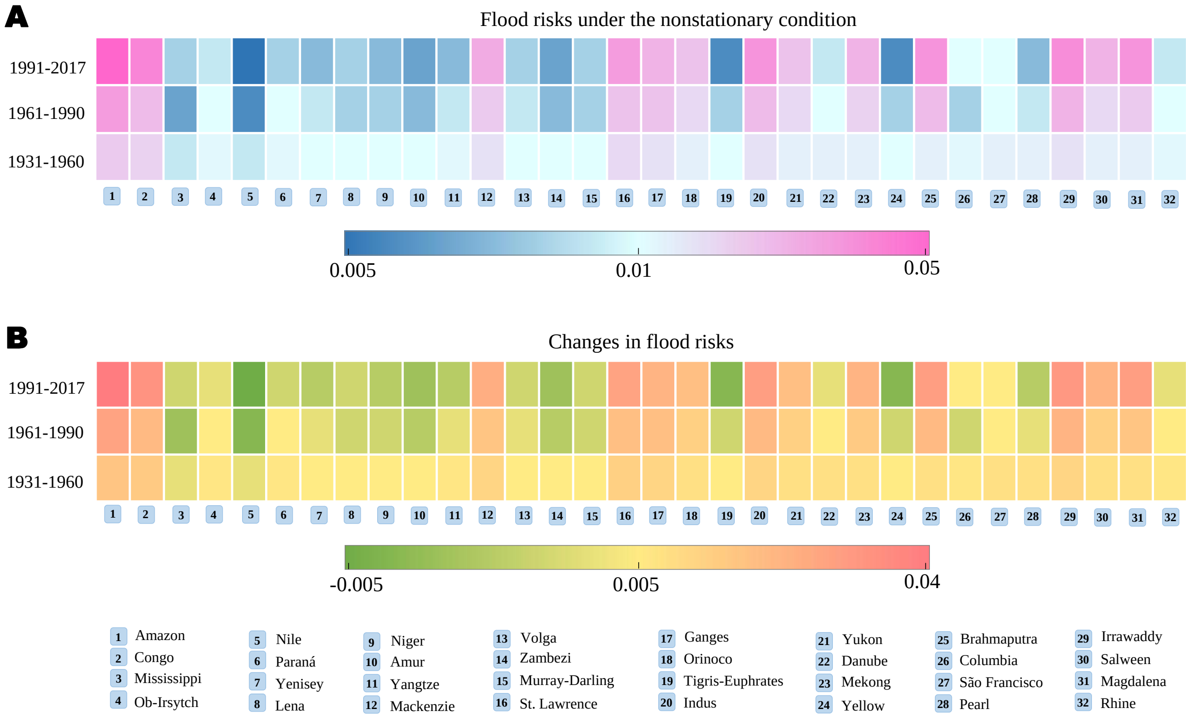

Fig. 9 Changes in flood risks in the world's 32 major rivers during three periods (1931-1960, 1961-1990, & 1991-2017). A. Flood risks under the nonstationary condition. B. Changes in flood risks between nonstationary and stationary conditions ($P(X \geqslant x) = 1\,\%$).

In sum, the integrated frequency analysis methodology proposed in this study aimed at exploring the multidecadal changes in climate and reservoir storage for assessing the nonstationarity in flood peaks and risks worldwide. The results demonstrated that the proposed method not only can adequately identify the contribution of climatic and anthropogenic factors to the nonstationarity in flood peaks but also can effectively quantify the changes in flood risks by modeling the time-varying characteristics in the distribution of flood peaks. This study opens up new perspectives on expanding current knowledge of the nonstationary flood frequency analysis while bringing novel statistical tools to the analysis of hydroevents for improving policy and construction recommendations by collaborating original thinking and scientific renewal.

5. Conclusions

This study conducted a holistic assessment of the changing climate and reservoir storage on the nonstationarity of flood peaks and risks worldwide by an integrated frequency analysis approach. For the flood risk analysis, the stationary frequency analysis served as the benchmark. The main conclusions were drawn as follows.

The spatial patterns of flood trends were explicitly classified into three groups. Regional average flood peaks changed from +19.3%/decade to –31.6%/decade during 1961-2017, as compared with the average flood peaks over the baseline period of 1931-1960. The declining trends of flood peaks tended to be larger as the catchment size and reservoir storage increase. From a global standpoint, there are more observation stations with significant decreasing trends in flood peaks than with significant increasing trends over the datasets investigated.

Regarding the contribution to the nonstationarity of flood peaks, the largest increase in flood risks were generally associated with the largest increase in warm year probabilities whereas the largest decrease in flood risks were generally associated with the largest increase in the flood control capacity of reservoirs/dams. The strong responses implied that reservoir regulation and global warming had significant impacts on the nonstationarity of flood peaks and risks. Among the 32 major rivers, the risks of flooding from 5 rivers significantly increased (1%→5%) under the nonstationary condition in response to warming climate while the risks of flooding from 7 rivers largely reduced (1%→0.5%) under the nonstationary condition in response to reservoirs/dams regulation, as compared to those under the stationary condition over the historical period.

The identification and quantification of the nonstationarity in flood peaks and risks highlighted the benefits of the nonstationary frequency analysis to social infrastructure planning and designing as well as water resources management in the best interest of social sustainability. Nonstationarity of flood peaks may also arise due to small interventions or extractions at various places in one basin. Each of these interventions or extractions may be small, but their cumulative impact could be significant. Future research could be centered on quantifying the impacts of large-scale atmospheric and oceanic mechanisms, oscillations, land-surface changes and irrigation intensifications on the nonstationarity of flood peaks and risks, given that more climatic and anthropogenic changes would affect river systems.

Acknowledgments

This work was supported by the Research Council of Norway (FRINATEK Project 274310) and the National Natural Science Foundation of China (No. 51539009, 51538173 and No. U1865201). The author thanks the GRDC for providing river streamflow data and thanks the NCDC and the WMO for providing GSOD data. The author also thanks the NASA and the FAO of the United Nations for providing dam and reservoir data. The authors would like to thank the Editors and anonymous Reviewers for their constructive comments that greatly enrich the manuscript.

References

Arheimer, B., Donnelly, C., & Lindström, G., 2017. Regulation of snow-fed rivers affects flow regimes more than climate change. Nat. Commun. 8, 62.

Ashraf, F. B., Haghighi, A. T., Riml, J., Alfredsen, K., Koskela, J. J., Kløve, B., & Marttila, H., 2018. Changes in short term river flow regulation and hydropeaking in Nordic rivers. Sci. Rep. 8, 17232.

Aissia, M. A. B., Chebana, F., Ouarda, T. B., Roy, L., Bruneau, P., & Barbet, M., 2014. Dependence evolution of hydrological characteristics, applied to floods in a climate change context in Quebec. J. Hydrol. 519, 148-163.

Barichivich, J., Gloor, E., Peylin, P., Brienen, R. J., Schöngart, J., Espinoza, J. C., & Pattnayak, K. C. Recent intensification of Amazon flooding extremes driven by strengthened Walker circulation. Sci. Adv. 4, 8785 (2018).

Best, J., 2019. Anthropogenic stresses on the world's big rivers. Nat. Geosci. 12, 7-21.

Blöschl, G., Hall, J., Parajka, J., et al., 2017. Changing climate shifts timing of European floods. Science 357, 588-590.

Blöschl, G., Hall, J., Viglione, A., et al., 2019. Changing climate both increases and decreases European river floods. Nature 573, 108-111.

Blöschl, G., Kiss, A., Viglione, A. et al., 2020. Current European flood-rich period exceptional compared with past 500 years. Nature 583, 560-566.

Cheng, L., & AghaKouchak, A., 2014. Nonstationary precipitation intensity-duration-frequency curves for infrastructure design in a changing climate. Sci. Rep. 4, 7093.

Chebana, F., Ouarda, T. B., & Duong, T. C., 2013. Testing for multivariate trends in hydrologic frequency analysis. J. Hydrol. 486, 519-530.

Do, H. X., Westra, S., & Leonard, M., 2017. A global-scale investigation of trends in annual maximum streamflow. J. Hydro. 28-43.

Dottori, F., Szewczyk, W., Ciscar, J. C., Zhao, F., Alfieri, L., Hirabayashi, Y., & Feyen, L., 2018. Increased human and economic losses from river flooding with anthropogenic warming. Nat. Clim. Change 8, 781.

De Koning, K., Filatova, T., Need, A., & Bin, O., 2019. Avoiding or mitigating flooding: Bottom-up drivers of urban resilience to climate change in the USA. Global Environ. Change 59, 101981.

Fraser, A. M., and H. L. Swinney., 1986. Independent coordinates for strange attractors from mutual information, Phys. Rev. A. 33(2), 1134-1140.

Forzieri, G., Bianchi, A., e Silva, F. B., Herrera, M. A. M., Leblois, A., Lavalle, C., & Feyen, L., 2018. Escalating impacts of climate extremes on critical infrastructures in Europe. Global Environ. Change 48, 97-107.

Frolova, N. L., Kireeva, M. B., Magrickiy, D. V., et al., 2017. Hydrological hazards in Russia: origin, classification, changes and risk assessment. Nat. Hazards 88, 103-131.

GRDC, 2020. WMO Basins and Sub-Basins / Global Runoff Data Centre, GRDC. 3rd, rev. ext. ed. Koblenz, Germany: Federal Institute of Hydrology (BfG).

Gao, L., Tao, B., Miao, Y., et al., 2019. A global data set for economic losses of extreme hydrological events during 1960 - 2014. Water Resour. Res. 55, 5165-5175.

Gernaat, D. E., Bogaart, P. W., van Vuuren, D. P., Biemans, H., & Niessink, R., 2017.

High-resolution assessment of global technical and economic hydropower potential. Nat. Energy 2, 821.

Gottschalk, L., Yu, K. X., Leblois, E., & Xiong, L., 2013. Statistics of low flow: Theoretical derivation of the distribution of minimum streamflow series. J. Hydrol. 481, 204-219.

Güneralp, B., Güneralp, İ., & Liu, Y., 2015. Changing global patterns of urban exposure to flood and drought hazards. Global Environ. Change 31, 217-225.

Haer, T., Husby, T. G., Botzen, W. W., & Aerts, J. C., 2020. The safe development paradox: An agent-based model for flood risk under climate change in the European Union. Global Environ. Change 60, 102009.

Haddeland, I., Heinke, J., Biemans, H., Eisner, S., Florke, M., Hanasaki, N., et al., 2014. Global water resources affected by human interventions and climate change. Proc. Natl. Acad. Sci. U. S. A. 111, 3251-3256.

Hall, J., & Blöschl, G., 2018. Spatial patterns and characteristics of flood seasonality in Europe. Hydrol. Earth Syst. Sci. 22, 3883-3901.

Hirabayashi, Y., Mahendran, R., Koirala, S., Konoshima, L., Yamazaki, D., Watanabe, S., & Kanae, S., 2013. Global flood risk under climate change. Nat. Clim. Change 3, 816.

Hodgkins, G. A., Whitfield, P. H., Burn, D. H., et al., 2017. Climate-driven variability in the occurrence of major floods across North America and Europe. J. Hydrol. 552, 704-717.

Hudson, P., Botzen, W. W., & Aerts, J. C., 2019. Flood insurance arrangements in the

European Union for future flood risk under climate and socioeconomic change. Global Environ. Change 58, 101966.

Hui, R., Herman, J. D., Lund, J. R., & Madani, K., 2018. Adaptive water infrastructure planning for nonstationary hydrology. Adv. Water Resour. 83-94.

Huss, M., & Hock, R., 2018. Global-scale hydrological response to future glacier mass loss. Nat. Clim. Change 8(2), 135-140.

Jones, R. H., Westra, S., & Sharma, A., 2010. Observed relationships between extreme sub-daily precipitation, surface temperature, and relative humidity. Geophys. Res. Lett. 37(22).

Koutsoyiannis, D., 2006. Nonstationarity versus scaling in hydrology: J. Hydrol. 324, 239-254.

Krueger, E., Rao, P. S. C., & Borchardt, D., 2019. Quantifying urban water supply security under global change. Global Environ. Change 56, 66-74.

Lehner, B., C. Reidy Liermann, C. Revenga, C. Vörösmarty, B. Fekete, P. Crouzet, P. Döll, M. Endejan, K. Frenken, J. Magome, C. Nilsson, J.C. Robertson, R. Rodel, N. Sindorf, and D. Wisser., 2011. High-resolution mapping of the world's reservoirs and dams for sustainable river-flow management. Front. Ecol. Environ. 9, 494-502.

Lehner, B., Grill G., 2013. Global river hydrography and network routing: baseline data and new approaches to study the world’s large river systems. Hydrol. Processes 27(15), 2171-2186.

Lehner, B., 2013. HydroSHEDS technical documentation, version 1.2. World Wildlife

Fund US, 1-25.

Li, J., Liu, X., & Chen, F., 2015. Evaluation of nonstationarity in annual maximum flood series and the associations with large-scale climate patterns and human activities. Water Resour. Manage. 29(5), 1653-1668.

Lins, H.F., and T.A. Cohn, 2011. Stationarity: Wanted dead or alive?. J. Am. Water Resour. Assoc. 47, 475-480.

Liang, Z., Yang, J., Hu, Y., Wang, J., Li, B., & Zhao, J., 2018. A sample reconstruction method based on a modified reservoir index for flood frequency analysis of non-stationary hydrological series. Stoc. Environ. Res. Risk Assess. 32, 1561-1571.

Mangini, W., Viglione, A., Hall, J., et al., 2018. Detection of trends in magnitude and frequency of flood peaks across Europe. Hydrol. Sci. J. 63, 493-512.

Mallakpour, I., & Villarini, G., 2015. The changing nature of flooding across the central United States. Nat. Clim. Change 5, 250.

Milly, P. C., Betancourt, J., Falkenmark, M., Hirsch, R. M., Kundzewicz, Z. W., Lettenmaier, D. P., & Stouffer, R. J., 2008. Stationarity is dead: Whither water management?. Science 319, 573-574.

Milly, P. C., Dunne, K. A., & Vecchia, A. V., 2005. Global pattern of trends in streamflow and water availability in a changing climate. Nature 438, 347-350.

Mishra, V., Wallace, J. M., & Lettenmaier, D. P., 2012. Relationship between hourly extreme precipitation and local air temperature in the United States. Geophys. Res. Lett. 39(16).

Montanari, A., Young, G., Savenije, H. H. G., Hughes, D., Wagener, T., Ren, L. L., & Blöschl, G., 2013. “Panta Rhei—everything flows”: change in hydrology and society—the IAHS scientific decade 2013–2022. Hydrol. Sci. J. 58, 1256-1275.

Musselman, K. N., Lehner, F., Ikeda, K., Clark, M. P., Prein, A. F., Liu, C., & Rasmussen, R., 2018. Projected increases and shifts in rain-on-snow flood risk over western North America. Nat. Clim. Change 8, 808.

Nilsson, C., Reidy, C. A., Dynesius, M., & Revenga, C., 2005. Fragmentation and flow regulation of the world's large river systems. Science 308, 405-408.

Najibi, N., & Devineni, N., 2018. Recent trends in the frequency and duration of global floods. Earth Syst. Dynam. 9, 757-783.

Ouarda, T. B., & Charron, C., 2018. Nonstationary temperature-duration-frequency curves. Sci. Rep. 8, 15493.

Paprotny, D., Sebastian, A., Morales-Nápoles, O., & Jonkman, S. N., 2018. Trends in flood losses in Europe over the past 150 years. Nat. Commun. 9, 1985.

Rigby, R. A., & Stasinopoulos, D. M., 2005. Generalized additive models for location, scale and shape. J. R. Stat. Soc. 54, 507-554.

Sarhadi, A., Ausín, M. C., Wiper, M. P., Touma, D., & Diffenbaugh, N. S., 2018. Multidimensional risk in a nonstationary climate: Joint probability of increasingly severe warm and dry conditions. Sci. Adv. 4, 3487.

Schaller, N., Kay, A. L., Lamb, R., Massey, N. R., Van Oldenborgh, G. J., Otto, F. E., & Bowery, A., 2016. Human influence on climate in the 2014 southern England winter floods and their impacts. Nat. Clim. Change 6, 627.

Schilling, K. E., Chan, K. S. , Liu, H. , & Zhang, Y. K., 2015. Quantifying the effect of land use land cover change on increasing discharge in the upper mississippi river. J. Hydrol. 387, 343-345.

Serago JM., Vogel RM., 2018. Parsimonious nonstationary flood frequency analysis. Adv. Water Resour. 112, 1-16.

Sharma, A., 2000. Seasonal to interannual rainfall probabilistic forecasts for improved water supply management: Part 1-A strategy for system predictor identification. . J. Hydrol. 239(1-4), 232-239.

Sharma, A. and R. Mehrotra., 2014. An information theoretic alternative to model a natural system using observational information alone. Water Resour. Res. 50, 650-660.

Sharma, A., R. Mehrotra, J. Li and S. Jha., 2016. A programming tool for nonparametric system prediction using Partial Informational Correlation and Partial Weights. Environ. Modell. Software 83, 271-275.

Sharma, A., Wasko, C., & Lettenmaier, D. P., 2018. If precipitation extremes are increasing, why aren't floods?. Water Resour. Res. 54(11), 8545-8551.

Strupczewski, W. G., Singh, V. P., & Feluch, W., 2001. Non-stationary approach to at-site flood frequency modelling I. Maximum likelihood estimation. J. Hydrol. 248, 123-142.

Son, C., Lee, T., & Kwon, H. H., 2017. Integrating nonstationary behaviors of typhoon and non-typhoon extreme rainfall events in East Asia. Sci. Rep. 7, 5097.

Sun, P., Wen, Q., Zhang, Q., Singh, V. P., Sun, Y., & Li, J., 2018.

Nonstationarity-based evaluation of flood frequency and flood risk in the Huai River basin, China. J. Hydrol. 567, 393-404.

Tanoue, M., Hirabayashi, Y., & Ikeuchi, H., 2016. Global-scale river flood vulnerability in the last 50 years. Sci. Rep. 6, 36021.

Villarini, G., Serinaldi, F., Smith, J. A., & Krajewski, W. F., 2009. On the stationarity of annual flood peaks in the continental United States during the 20th century. Water Resour. Res. 45(8): 1-17.

Villarini, G., Smith, J. A., Serinaldi, F., Ntelekos, A. A., & Schwarz, U., 2011. Analyses of extreme flooding in Austria over the period 1951-2006. Int. J. Climatol. 32(8): 1178-1192.

Villarini, G., & Strong, A., 2014. Roles of climate and agricultural practices in discharge changes in an agricultural watershed in Iowa. Agric. Ecosyst. Environ. 188, 204-211.

Vogel, R.M., Yaindl, C., Walter, M., 2011. Nonstationarity: flood magnification and recurrence reduction factors in the United States1. J. Am. Water Resour. Assoc. 47, 464-474.

Wasko, C., & Sharma, A., 2017. Global assessment of flood and storm extremes with increased temperatures. Sci. Rep. 7(1).

Wasko, C., Sharma, A., & Lettenmaier, D. P., 2019. Increases in temperature do not translate to increased flooding. Nat. Commun. 10(1), 1-3.

Winsemius, H. C., Aerts, J. C., van Beek, L. P., et al., 2016. Global drivers of future river flood risk. Nat. Clim. Change 6, 381.

Willner, S. N., Otto, C., & Levermann, A., 2018. Global economic response to river floods. Nat. Clim. Change 8, 594.

Wu, X., Guo, S., Yin, J., Yang, G., Zhong, Y., & Liu, D., 2018. On the event-based extreme precipitation across China: Time distribution patterns, trends, and return levels. J. Hydrol. 562, 305-317.

WWF, 2019. HydroRivers, World Wildlife Fund. Data online available at www.hydrosheds.org. Online received in February 2020.

Xiong, B., Xiong, L., Chen, J., Xu, C. Y., & Li, L., 2018. Multiple causes of nonstationarity in the Weihe annual low-flow series. Hydrol. Earth Syst. Sci. 22, 1525-1542.

Yan L, Xiong L, Guo S, Xu CY, Xia J, Du T., 2017. Comparison of four nonstationary hydrologic design methods for changing environment. J. Hydrol. 551, 132-150.

Yin, J., Gentine, P., Zhou, S., Sullivan, S. C., Wang, R., Zhang, Y., & Guo, S., 2018. Large increase in global storm runoff extremes driven by climate and anthropogenic changes. Nat. Commun. 9(1).

Yu, G., Wright, D. B., Zhu, Z., Smith, C., & Holman, K. D., 2019. Process-based flood frequency analysis in an agricultural watershed exhibiting nonstationary flood seasonality. Hydrol. Earth Syst. Sci. 23, 2225-2243.

Zhou, T., Nijssen, B., Gao, H., & Lettenmaier, D. P., 2016. The contribution of reservoirs to global land surface water storage variations. J. Hydrometeorol 17, 309-325.

***Declaration of Interest Statement**

Declaration of interests

☒ The authors declare that they have no known competing financial interests or personal relationships that could have appeared to influence the work reported in this paper.

☐The authors declare the following financial interests/personal relationships which may be considered as potential competing interests: